

Unconventional magnetic response of clean interface superconductors with strong Rashba spin-orbit coupling

Daniel F. Agterberg,¹ Egor Babaev,^{2,3} and Julien Garaud^{3,2}

¹*Department of Physics, University of Wisconsin-Milwaukee, Milwaukee, WI 53211*

²*Department of Theoretical Physics, Royal Institute of Technology, Stockholm, SE-10691 Sweden*

³*Department of Physics, University of Massachusetts Amherst, MA 01003 USA*

The magnetic response of superconductors is determined by the properties of topological excitations. For more than a half-century, experiments have observed various configurations of Abrikosov vortices, which are the simplest defects of a $S^1 \rightarrow S^1$ topological map. In principle, theory allows for multicomponent systems with flux-carrying topological excitations different from Abrikosov vortices. However, in practice, largely due to electromagnetic and other intercomponent interactions, such defects are very rare in superconducting systems. Here we demonstrate microscopically, that interface superconductors, such as $\text{SrTiO}_3/\text{LaAlO}_3$, in the clean limit with a strong Rashba spin-orbit coupling make ideal candidates to observe an unconventional magnetic response where the flux-carrying objects are skyrmions of $S^2 \rightarrow S^2$ topological maps.

A class of systems where unusual vortex physics is important is superfluids and superconductors that break transitional symmetry, such as predicted to appear in spin-orbit coupled Bose-Einstein condensates [1–3], Fulde Ferrell Larkin Ovchinnikov (FFLO) and related states [4–8], quantum crystals [9, 10], and pair density wave superfluids/superconductors [11–13]. These systems allow fractional vortices. Such vortices belong to the same $S^1 \rightarrow S^1$ topological map as conventional vortices and can give rise to interesting physical consequences such as paired superfluids and charge 4 and charge 6 superconductors [8, 13–16]. However, fractional vortices are energetically more expensive than integer-flux vortices and thus are typically excluded from the magnetic response under normal conditions. A different class of states is theoretically possible when the minimum energy excitation is neither a fractional nor an integer-flux vortex, but a skyrmion. Skyrmions can be visualized as states in which pairs of fractional vortices have a preferred separation. As discussed in detail below, such configurations are distinct topologically since they are characterized by a $S^2 \rightarrow S^2$ topological map. Although the existence of such states in superconductors can be justified by symmetry-based arguments, they have not been experimentally observed nor do they have a microscopic basis. Here we give such a microscopic basis. In particular, we show that in clean two-dimensional (2D) superconductors with strong Rashba spin-orbit coupling, such flux-carrying defects are ubiquitous in a FFLO-like phase. This theory applies to two-dimensional (2D) interface superconductors, such as that which appears at the interface of SrTiO_3 and LaAlO_3 [17, 18]. The field of 2D superconductors has grown tremendously over recent years with the discovery of electric field induced superconductivity in SrTiO_3 [19], KTaO_3 [20], and MoS_2 [21, 22]. This growing set of materials present an ideal experimental opportunity to examine the unconventional magnetic response of skyrmions.

We consider a weak-coupling theory for a clean superconductor with isotropic pairing interactions (s -wave

pairing), a strong Rashba spin-orbit coupling, and an in-plane Zeeman field. We consider the chemical potential to be well above the Dirac point, away from the limit at which Majorana modes are predicted. For a wide range of in-plane fields and temperatures, we show there exists a phase akin to the FFLO phase that we call the multiple- Q phase [6, 23]. We show that the phase boundary for the multiple- Q phase is well described by a Ginzburg Landau (GL) theory derived from this weak coupling theory. Using this GL theory, we find our central result: fractional vortices and skyrmions (split-core vortices) are prevalent in the multiple- Q phase when a magnetic field is applied perpendicular to the plane. Prior to giving the details of the microscopic theory, we provide a summary of the phenomenological $U(1) \times U(1)$ theory that admits fractional vortices and skyrmions as possible topological excitations. We further show that the multiple- Q phase must also exhibit unconventional type-1.5 superconductivity in a region of the phase diagram. This results in coalescence and formation of vortex aggregates surrounded by vortexless regions.

Fractional vortices and skyrmions in $U(1) \times U(1)$ theories. The GL theory for the order parameter, derived below, takes the form

$$F = \int d^2x \left\{ \frac{1}{2} B^2 - H_z B + \beta_m |\Delta_q|^2 |\Delta_{-q}|^2 + \sum_{i=x,y} \kappa_{1i} |D_i \Delta_q|^2 + \alpha_1 |\Delta_q|^2 + \frac{\beta_1}{2} |\Delta_q|^4 + \sum_{i=x,y} \kappa_{2i} |D_i \Delta_{-q}|^2 + \alpha_2 |\Delta_{-q}|^2 + \frac{\beta_2}{2} |\Delta_{-q}|^4 \right\}, \quad (1)$$

where $D_j = \partial_j + 2ieA_j$, $B = \partial_x A_y - \partial_y A_x$, and H_z is the applied field normal to the interface. $\Delta_{\pm q} = |\Delta_{\pm q}| e^{i\varphi_{\pm}}$ are complex fields representing the superconducting condensates. The free energy has a $U(1) \times U(1)$ invariance. In the context of the microscopic theory discussed below, one $U(1)$ symmetry is the usual gauge invariance while the second $U(1)$ symmetry stems from translational in-

variance. Depending on the parameters $\alpha_1, \beta_1, \alpha_2, \beta_2$ and β_m of the interacting potential, there can be three homogeneous ground states. Two of these we name the single- Q phase, in which either $\Delta_q = 0$ or $\Delta_{-q} = 0$, and the third is the multiple- Q phase (occurring when $\beta_1\beta_2 > \beta_m^2$ and $\alpha_1, \alpha_2 < 0$) for which both $\Delta_q \neq 0$ and $\Delta_{-q} \neq 0$. There are two different coherence lengths ξ_{\pm} . These can be uniquely associated with the condensates $\Delta_{\pm q}$ in the single- Q phase. In the multiple- Q phase, these two coherence lengths describe linear combinations of $\Delta_{\pm q}$. $\xi_+ < \xi_-$ for the entire range of parameters and ξ_- diverges at the single- Q to multiple- Q transition (see details in Appendix B).

The parameters α 's, β 's and κ 's of the model are microscopically determined and e , which is used to parametrize the penetration depth of the magnetic field, is the only free parameter of the GL free energy Eq. 1. Because of the $U(1) \times U(1)$ symmetry, both condensates are independently conserved. This implies that, in general, there are two independent second critical fields $H_{c2}^{(-q)} < H_{c2}^{(q)}$ associated with the (independent) destruction of the condensates.

The elementary topological excitations here are fractional vortices. That is, field configurations with independent 2π windings in either $\Delta_{\pm q}$ (e.g. φ_+ has $\oint \nabla \varphi_+ = 2\pi$ winding while $\oint \nabla \varphi_- = 0$). Configurations with winding n in Δ_q and m in Δ_{-q} , denoted (n, m) , carry a flux that is not necessarily an integer multiple of the flux quantum $\Phi_0 = 2\pi/e$ [24]

$$\Phi_{n,m} = \frac{n\kappa_{1x}|\Delta_q|^2 + m\kappa_{2x}|\Delta_{-q}|^2}{\kappa_{1x}|\Delta_q|^2 + \kappa_{2x}|\Delta_{-q}|^2} \Phi_0. \quad (2)$$

In the single- Q phase, where only one component condenses, the flux carried is always an integer multiple of Φ_0 . In the multiple- Q phase, each component Δ_q and Δ_{-q} respectively carries $\Phi_{1,0}$ and $\Phi_{0,1}$, fractions of the flux quantum. When both condensates have the same winding $m = n$, both these fractions add up to an integer multiple of Φ_0 . The corresponding configurations are n 'composite' vortices, each carrying one flux quantum. These have finite energy per unit length (independent of system size) due to screened currents. When there are fractional vortices, that is when $m \neq n$, there are unscreened counter-currents in both components. This leads to logarithmically divergent energy per unit length, making their creation in the bulk unlikely. Nevertheless, fractional vortices can be thermodynamically stable near boundaries [25].

Typically, a $U(1) \times U(1)$ superconductor in an external field forms composite vortices with $(1, 1)$ winding due to the logarithmic attraction of fractional $(1, 0)$ and $(0, 1)$ vortices. Winding in the relative phase $\varphi_r = \varphi_+ - \varphi_-$ signals fractional vortices. That is, local 2π winding in φ_r signals non overlapping cores of fractional vortices in both condensates. This can be due to either fractional vortices or to split-core vortices, skyrmions, as discussed below. Although two-component superconductors

are common, the associated skyrmions are usually unstable and decay into Abrikosov vortices. We show below that in the multiple- Q phase of the microscopic theory, skyrmions commonly appear in an external field.

Microscopic formulation. We consider the following Hamiltonian:

$$\mathcal{H} = \sum_{\mathbf{k}, \sigma} a_{\mathbf{k}\sigma}^\dagger \xi_{\mathbf{k}} a_{\mathbf{k}\sigma} + \sum_{\mathbf{k}\sigma\sigma'} a_{\mathbf{k}\sigma}^\dagger [\alpha \mathbf{g}_{\mathbf{k}} + \mu_B \mathbf{H}] \cdot \boldsymbol{\sigma}_{\sigma\sigma'} a_{\mathbf{k}\sigma'} + \frac{1}{2} V \sum_{\mathbf{k}, \mathbf{k}', \mathbf{q}} a_{\mathbf{k}+\mathbf{q}\uparrow}^\dagger a_{-\mathbf{k}+\mathbf{q}\downarrow}^\dagger a_{-\mathbf{k}'+\mathbf{q}\downarrow} a_{\mathbf{k}'+\mathbf{q}\uparrow} \quad (3)$$

where $a_{\mathbf{k}\sigma}$ are the annihilation operators with momentum \mathbf{k} and with pseudospin σ , $\xi_{\mathbf{k}} = \epsilon_{\mathbf{k}} - \mu$, $\mathbf{g}_{\mathbf{k}} = (k_y, -k_x)/k_F$ is the Rashba spin-orbit coupling, \mathbf{H} is an in-plane Zeeman field, $\epsilon_{\mathbf{k}} = k^2/(2m)$, and V is the s -wave pairing interaction. We assume a large Rashba spin-orbit coupling, so that $T_c, |\mu_B \mathbf{B}| \ll |\alpha|$. We ignore terms of the order $(\mu_B |\mathbf{B}|/\alpha)^2$, this limit considerably simplifies the theory. Helicity annihilation operators $a_{\mathbf{k}\pm}$ that represent the eigenstates of the single-particle Hamiltonian, annihilate particles in the two spin-dependent bands with energies $E_{\mathbf{k},\pm} = \epsilon(\mathbf{k}) \pm \alpha |\mathbf{g}_{\mathbf{k}}|$. The theory in the helicity basis is akin to a two-band theory for which we can follow standard methods to find the corresponding Eilenberger equations that describe the weak-coupling limit [26, 27]. This limit assumes $k_B T_c \ll \omega_c \ll \epsilon_F$ and $1/k_F \xi_0 \ll 1$ where T_c is the transition temperature, ω_c is the cut-off frequency, $\epsilon_F = \hbar^2 k_F^2/2m$ is the Fermi energy, and ξ_0 is zero-temperature superconducting coherence length. We provide details of the microscopic theory in Appendix A and present the main results here. Note that the assumption of s -wave pairing requires that the two gap functions (one for each helicity band) are equal at every point in space. We describe these two gap functions by the single gap function $\Delta(\mathbf{x})$. Prior to proceeding, it is useful to define δN which plays a central role in the theory. δN quantifies the difference in the density of states on the two Fermi surfaces associated with different helicity, it is defined as

$$\delta N = \frac{N_+ - N_-}{N_+ + N_-} = \frac{\alpha}{2\epsilon_F}. \quad (4)$$

Phase diagram for in-plane fields. We consider a field along the \hat{y} direction. Phenomenological arguments imply that $\Delta(\mathbf{x}) = \Delta_q e^{iqx}$ close to normal to superconducting transition [28]. We have examined the stability of this single- Q solution within the microscopic theory discussed above. In particular, we have minimized the microscopic free energy with respect to q and Δ_q . Once the optimal single- Q solution has been found we then set $\Delta(\mathbf{x}) = \Delta_q e^{iqx} + \Delta_{-q} e^{-iqx} + \Delta_{3q} e^{i3qx}$ and expand the free energy to quadratic order in Δ_{-q} and Δ_{3q} . If this additional contribution lowers the free energy, then the multiple- Q phase is stable. Our approach agrees with earlier calculations done for $\delta N = 0$ [6]. For $\delta N < 0.25$, we find that the phase diagram generically contains both single- Q and multiple- Q phases and resembles that shown

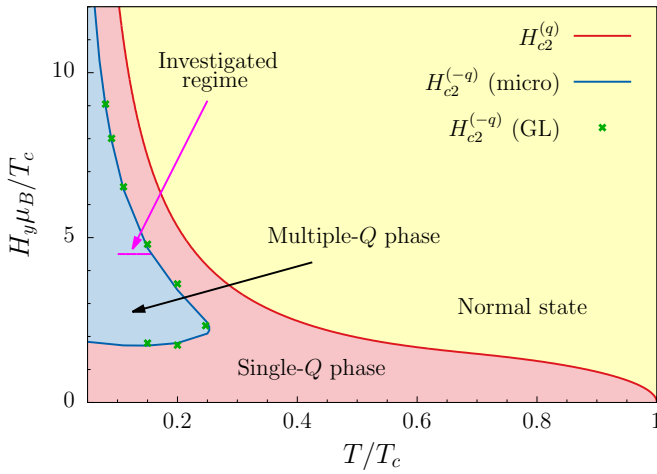


FIG. 1. The temperature-magnetic field phase diagram for a s -wave superconductor with $\delta N = 0.05$ (for in-plane magnetic fields). The line $H_{c2}^{(q)}$ denotes the transition from the normal phase to single- Q superconductor. The line $H_{c2}^{(-q)}$ (micro) denote the multiple- Q to single- Q phase transition found using the microscopic theory described in the text. The green crosses denote this same transition within the Ginzburg-Landau approximation of the microscopic theory. The line labelled "Investigated regime" is where we examined the role of an out of plane magnetic field.

in Fig. 1. For $\delta N \geq 0.25$, we find only the single- Q phase is stable. We have also derived the GL free energy of Eq. (1) from the microscopic theory ignoring Δ_{3q} (which numerically is found to be small). As shown in Fig. 1, this GL theory predicts a single- Q to multiple- Q phase boundary that is in good agreement with the full microscopic theory.

To address the response of the system to applied field H_z , we minimize the microscopically derived free energy (1) for decreasing temperatures (for details, see Appendix D). Below, unless otherwise specified, the magnetic field B is given in units of $H_{c2}^{(q)}$, and the condensate densities in units of their ground state. The spatial coordinates x and y are scaled in units $\sqrt{2\kappa_{1x}}$ and $\sqrt{2\kappa_{1y}}$ respectively. Additionally, the in-plane Zeeman field is fixed to be $H_y \mu_B / T_c = 4.5$ and $\delta N = 0.05$.

Skyrmions and fractional vortices. When λ is the largest length scale ($\lambda \gtrsim \xi_+, \xi_-$), depending on the applied field H_z , we find an unusual magnetic response featuring skyrmions. The smoking gun of this unconventional state already manifests in low applied fields, featuring the formation of thermodynamically stable fractional vortices near the boundary (see Fig. 2). The mechanism for the stabilization of these boundary fractional vortices [25] can be understood as follows. The condition that no current flows through the boundary is akin to placing an image fractional anti-vortex outside the superconductor. The fractional vortex/anti-vortex pair does not have a logarithmically divergent energy. Moreover, fractional vortices in Δ_{-q} experience a smaller Bean Livingston-like barrier than vortices in Δ_q . Consequently, these fractional vortices have the lowest field for entry into the superconductor. However, because they

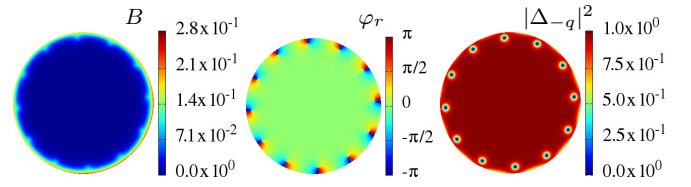


FIG. 2. (Color online) – Stable fractional vortices near boundaries. Vortices enter in the Δ_{-q} condensate, while no vortices enter in Δ_q . This can be seen from the phase difference, where winding in φ_r indicates the existence of fractional vortices.

have logarithmically divergent energy in the bulk, they cannot deeply penetrate into the superconductor. To compromise between the vortex/(image)anti-vortex attraction and repulsion due to Meissner current, the fractional vortices sit at a preferred finite distance from the boundary [25].

For higher values of the external field, vortices in Δ_q also overcome the Bean-Livingston barrier and start penetrating into the bulk. This results in formation of skyrmions which can coexist with near-boundary fractional vortices. At high fields, as shown in Fig. 3, lattices of vortices with split cores (as revealed by local winding in φ_r) are formed. The density-density interaction term, controlled by β_m , is responsible for this core-split vortices. These split-core vortices, the skyrmions, carry integer flux and have finite energy. Moreover, because their cores are split, skyrmions are characterized by an additional invariant due to the non-trivial homotopy $\pi_2(S^2) \in \mathbb{Z}$ of the $S^2 \rightarrow S^2$ topological maps. See details in Appendix B. Importantly, this extra invariant is zero for Abrikosov vortices. This topology also suggests the introduction of the pseudo-spin unit vector \mathbf{n} , defined by projecting the superconducting condensates onto Pauli matrices. Non-trivial texture of the pseudo-spin unequivocally indicates non-trivial topology of the $S^2 \rightarrow S^2$ map. Near the critical field $H_{c2}^{(-q)}$, that is, just below the single- Q to multiple- Q transition, two condensates form triangular lattices that are displaced with respect to each other. The displacement is such that vortices of Δ_{-q} lie in the center of a triangle of vortices in Δ_q . While the temperature is decreased, as in Fig. 3, vortices in Δ_{-q} no longer sit in the center of triangles of vortices in Δ_q . Vortices in Δ_{-q} pair with one of the three surrounding vortices of Δ_q and the resulting skyrmion lattice is no longer triangular. Further reducing the temperature induces stronger binding of the pairs that eventually merge to Abrikosov vortices, at the same time losing non-trivial features of the $S^2 \rightarrow S^2$ map. The resulting vortices form a usual triangular lattice (see additional material in Appendix C). Similar behaviour of the merging of the skyrmion lattice into Abrikosov lattice occurs at fixed temperature with decreasing fields. The core splitting strongly depends on the penetration depth. The larger λ (small e) is, the weaker the binding of fractional vortices becomes. Skyrmion lattices should

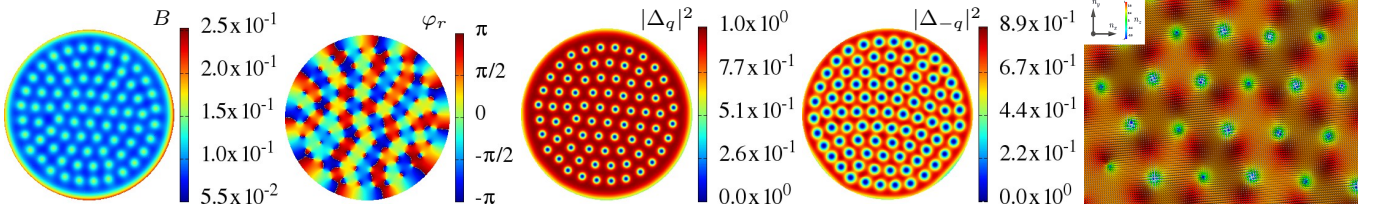


FIG. 3. (Color online) – Skyrmion lattice regime. This shows the magnetic field B , the relative phase between both condensates and their densities. The last panel displays the associated pseudo-spin (texture) \mathbf{n} obtained by projecting the superconducting condensates on Pauli matrices (see details in Appendix B). When the temperature is decreased, Δ_{-q} develops superconductivity with many vortices. In this regime, close to the critical field associated with Δ_{-q} , the lattice in Δ_{-q} does not coincide with that in Δ_q . This can be seen by the winding of the relative phase φ_r .

thus be easily identifiable in extreme type-2 superconductors.

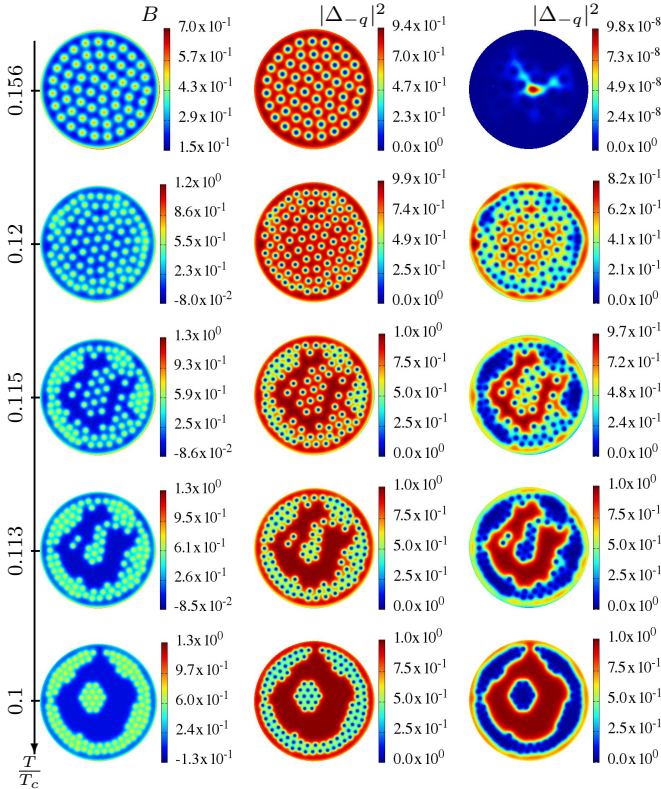


FIG. 4. (Color online) – Vortex aggregation at fixed field with cooling temperature. This shows the magnetic field B and the condensate densities. At $T/T_c = 0.156$, Δ_{-q} is completely suppressed, while Δ_q develops a triangular lattice up to some disclinations due the domain geometry (the disk cannot perfectly accommodate the lattice). As the temperature is decreased, Δ_{-q} develops superconductivity accompanied by vortices. When further cooled, vortices coalesce into clusters. The attraction between vortices is mediated by the (hybridized) coherence length ξ_- , which has longest range. The long-range attraction gets stronger as the system is cooled and vortex aggregates become very compact.

Type-1.5 Another highly unconventional feature that arises in microscopic theory of this system is associated with the fact that the coherence lengths ξ_- diverges at

the transition between single- Q and multiple- Q phase, while both the coherence length ξ_+ and the penetration depth λ remain finite (see Appendix B. Moreover if $\xi_+ < \lambda$, then there always exist a temperature range where $\xi_+ < \lambda < \xi_-$. Such a regime was recently termed “type-1.5” [29] and is a subject of great experimental interest [30]. In this regime, vortices are favoured over skyrmions. Interactions between vortices are non-monotonic long-range attractive and short-range repulsive [31, 32]. Due to the preferred intervortex separation, the usual Abrikosov lattice coalesces into vortex aggregates as shown in Fig. 4. At temperatures close to $T/T_c = 0.16$ (the single- Q to multiple- Q transition temperature when $H_z = 0$), the external field exceeds the second critical field $H_{c2}^{(-q)}$ of the second condensate and Δ_{-q} is completely suppressed. A moderate applied field nevertheless does not destroy Δ_q and it shows an hexagonal lattice of vortices. While the system is cooled, Δ_{-q} develops superconductivity accompanied with the formation of vortices. The disparity in length scales, leads to long-range attractive force between vortices. Initially, the attractive tail is rather weak and the effect on vortices is hardly noticeable. With further cooling, as Δ_{-q} increases, the attractive interaction becomes much stronger, seeding inhomogeneities in the vortex distribution to finally lead to segregation of clusters of vortices surrounded by regions of Meissner state. It is worth emphasizing here that clusters tend to sit near the boundary rather than in the bulk.

Our findings reveal that clean s -wave interface superconductors with strong Rashba spin-orbit coupling should exhibit novel and interesting physics under magnetic fields. The predicted skyrmion and fractional vortex formation and the behavior outside the usual type-1/type-2 dichotomy can be observable through either scanning SQUID or scanning tunnelling microscopy measurements. The observation of these effects will open a new window into the relationship between topological defects and magnetic response in superconductors.

We thank the Aspen Center for Physics where this work was initiated (NSF Grant No. 1066293). DFA acknowledges support from NSF grants No. DMR-0906655 and No. DMR-1335215. EB acknowledges support by the Knut and Alice Wallenberg Foundation through a

Royal Swedish Academy of Sciences Fellowship, by the Swedish Research Council, and by the National Science Foundation under the CAREER Award DMR-0955902. The computations were performed on resources provided by the Swedish National Infrastructure for Computing (SNIC) at National Supercomputer Center at Linköping, Sweden.

Appendix A: Derivation of the Ginzburg-Landau model

Using weak-coupling theory, the following GL free energy can be derived

$$F = \int d^2x \left\{ \alpha_1 |\Delta_q|^2 + \alpha_2 |\Delta_{-q}|^2 + \frac{\beta_1}{2} |\Delta_q|^4 + \frac{\beta_2}{2} |\Delta_{-q}|^4 + \beta_m |\Delta_q|^2 |\Delta_{-q}|^2 + \kappa_{1x} |D_x \Delta_q|^2 + \kappa_{2x} |D_x \Delta_{-q}|^2 + \kappa_{1y} |D_y \Delta_q|^2 + \kappa_{2y} |D_y \Delta_{-q}|^2 + \frac{1}{2} B_z^2 - H_z B_z \right\}. \quad (\text{A.1})$$

To do this, we define the usual Green's functions in Nambu space for each helicity band $\Psi_{\pm}^{\dagger}(\mathbf{R}) = [\psi_{\pm}^{\dagger}(\mathbf{R}), \psi_{\pm}(\mathbf{R})]$ and define the imaginary time Green's

function

$$\hat{G}_{\pm}(\mathbf{x}_1, \mathbf{x}_2; \tau_1 - \tau_2) = -\langle T_{\tau} \Psi_{\pm}(\mathbf{x}_1, \tau_1) \Psi_{\pm}^{\dagger}(\mathbf{x}_2, \tau_2) \rangle, \quad (\text{A.2})$$

here the operator T_{τ} arranges the field operators in ascending order of the imaginary time $0 < \tau < 1/T$ and $\Psi(\mathbf{x}, \tau) = e^{\tau \mathcal{H}} \Psi(\mathbf{x}) e^{-\tau \mathcal{H}}$. Introducing the center-of-mass coordinate, $\mathbf{R} = (\mathbf{x}_1 + \mathbf{x}_2)/2$, the relative coordinate, $\mathbf{r} = \mathbf{x}_1 - \mathbf{x}_2$, and performing the Fourier transform in the latter variable yields

$$\hat{G}_{\pm}(\mathbf{k}, \mathbf{R}; \omega_n) = \int d\mathbf{r} \int_0^{1/T} d\tau \hat{G}_{\pm}(\mathbf{x}_1, \mathbf{x}_2; \tau) e^{-i(\mathbf{k} \cdot \mathbf{r} - \omega_n \tau)}, \quad (\text{A.3})$$

where $\omega_n = (2n + 1)\pi T$ is the fermionic Matsubara frequency.

We define the quasi-classical Greens functions

$$\hat{g}_{\pm}(\hat{\mathbf{k}}, \mathbf{R}, \omega_n) = \begin{pmatrix} g_{\pm} & f_{\pm} \\ f_{\pm}^{\dagger} & -g_{\pm} \end{pmatrix} \equiv \frac{i}{\pi} \int d\xi \hat{\tau}_3 \hat{G}_{\pm}(\mathbf{k}, \mathbf{R}, \omega_n), \quad (\text{A.4})$$

where $d\xi$ integrates out the variable perpendicular to the Fermi surface, $\hat{\mathbf{k}}$ is vector on the Fermi surface, and τ_3 is the z -component of the Pauli matrices acting on the particle-hole space.

The standard quasi-classical approach [26, 27, 33] results in the following Eilenberger equations for this system (here we have assumed a small Zeeman field, that is we have kept terms up to order $\mu_B B/\alpha$):

$$[\omega_n \pm i\mu_B \hat{z} \cdot \mathbf{k} \times \mathbf{B} + \frac{1}{2} \mathbf{v}_{\hat{\mathbf{k}}} \cdot (\nabla - 2ie\mathbf{A})] f_{\pm} = \Delta_{\pm}(\hat{\mathbf{k}}, \mathbf{R}) g_{\pm} \quad (\text{A.5})$$

$$[\omega_n \pm i\mu_B \hat{z} \cdot \mathbf{k} \times \mathbf{B} - \frac{1}{2} \mathbf{v}_{\hat{\mathbf{k}}} \cdot (\nabla + 2ie\mathbf{A})] f_{\pm}^{\dagger} = \Delta_{\pm}^*(\hat{\mathbf{k}}, \mathbf{R}) g_{\pm} \quad (\text{A.6})$$

where $f_{\pm}^{\dagger} f_{\pm} + g_{\pm}^2 = 1$. The gap equation is

$$\Delta_i(\hat{\mathbf{k}}, \mathbf{R}) = \pi T \sum_{n,j} N_j \langle V_{ij}(\hat{\mathbf{k}}, \hat{\mathbf{k}}') f_j(\hat{\mathbf{k}}', \mathbf{R}, \omega_n) \rangle_{\hat{\mathbf{k}}'} \quad (\text{A.7})$$

where the effective pairing interaction is (with a finite Zeeman field, this remains correct up to order $(\mu_B |\mathbf{B}|/\alpha)^2$)

$$V = \frac{1}{2} V \begin{pmatrix} e^{i(\phi - \phi')} & e^{i(\phi + \phi')} \\ e^{-i(\phi + \phi')} & e^{-i(\phi - \phi')} \end{pmatrix} \quad (\text{A.8})$$

where $e^{i\phi} = (k_x + ik_y)/|\mathbf{k}|$. Redefining the gap functions $\Delta_{\pm}(\mathbf{k}, \mathbf{R}) = \pm e^{\pm i\phi} \tilde{\Delta}_{\pm}(\mathbf{k}, \mathbf{R})$ and the propagators $f_{\pm}(\mathbf{k}, \mathbf{R}, i\omega_n) = \pm e^{\pm i\phi} \tilde{f}_{\pm}(\mathbf{k}, \mathbf{R}, i\omega_n)$ yields simplified two-band Eilenberger equations. The gap functions can then be written as $\tilde{\Delta}_{\alpha}(\hat{\mathbf{k}}, \mathbf{R}) = \Delta_{\alpha}(\mathbf{R})$ and the gap equation implies that $\Delta_{+}(\mathbf{R}) - \Delta_{-}(\mathbf{R}) = 0$. In the following, we set $\Delta(\mathbf{R}) = \Delta_{+}(\mathbf{R}) = \Delta_{-}(\mathbf{R})$ and $f_{\alpha}(\hat{\mathbf{k}}, \mathbf{R}, \omega_n) = \tilde{f}_{\alpha}(\hat{\mathbf{k}}, \mathbf{R}, \omega_n)$.

The Eilenberger equations can be derived from a Gibbs free-energy functional [26]. Once the Eilenberger equations are solved for a given functional form of $\Delta(\mathbf{R})$ and

a known magnetic field, this free energy functional be- comes

$$\Omega_{\text{SN}} = \int d\mathbf{R} \left[V^{-1} |\Delta(\mathbf{R})|^2 - \pi T \sum_{n \geq 0, j} N_j \left\langle I_j(\hat{\mathbf{k}}, \mathbf{R}, \omega_n) + I_j^*(\hat{\mathbf{k}}, \mathbf{R}, \omega_n) \right\rangle \right], \quad (\text{A.9})$$

where N_j is the density of states on band j and

$$I_j(\hat{\mathbf{k}}, \mathbf{R}, \omega_n) = \frac{\Delta^*(\mathbf{R}) f_j(\hat{\mathbf{k}}, \mathbf{R}, \omega_n) + f_j^\dagger(\hat{\mathbf{k}}, \mathbf{R}, \omega_n) \Delta(\mathbf{R})}{1 + g_j(\hat{\mathbf{k}}, \mathbf{R}, \omega_n)}. \quad (\text{A.10})$$

Substituting $\Delta(\mathbf{R}) = \Delta_q e^{iqx} + \Delta_{-q} e^{-iqx}$ into the Eq. A.10 (this is for a field applied along \hat{y}) and keeping powers to fourth order in the order parameter components yields the following expressions for the parameters in GL free energy

$$\alpha_1 = \frac{1}{V} - 2\pi T \sum_{n \geq 0} \left\{ \frac{N_+}{\sqrt{\omega_n^2 + H_q^2}} + \frac{N_-}{\sqrt{\omega_n^2 + H_{-q}^2}} \right\} \quad (\text{A.11})$$

$$\alpha_2 = \frac{1}{V} - 2\pi T \sum_{n \geq 0} \left\{ \frac{N_-}{\sqrt{\omega_n^2 + H_q^2}} + \frac{N_+}{\sqrt{\omega_n^2 + H_{-q}^2}} \right\} \quad (\text{A.12})$$

$$\beta_1 = \frac{\pi T}{2} \sum_{n \geq 0} \left\{ N_+ \frac{2\omega_n^2 - H_q^2}{(\omega_n^2 + H_q^2)^{5/2}} + N_- \frac{2\omega_n^2 - H_{-q}^2}{(\omega_n^2 + H_{-q}^2)^{5/2}} \right\} \quad (\text{A.13})$$

$$\beta_2 = \frac{\pi T}{2} \sum_{n \geq 0} \left\{ N_- \frac{2\omega_n^2 - H_q^2}{(\omega_n^2 + H_q^2)^{5/2}} + N_+ \frac{2\omega_n^2 - H_{-q}^2}{(\omega_n^2 + H_{-q}^2)^{5/2}} \right\} \quad (\text{A.14})$$

$$\beta_m = 2\pi T \frac{(N_+ + N_-)}{qv_F} \sum_{n \geq 0} \left\{ \frac{(2\omega_n^2 + H_q^2)H_q}{\omega_n^2(\omega_n^2 + H_q^2)^{3/2}} + \frac{(2\omega_n^2 + H_{-q}^2)H_{-q}}{\omega_n^2(\omega_n^2 + H_{-q}^2)^{3/2}} \right\} \quad (\text{A.15})$$

$$\kappa_{1x} = \frac{\pi T}{8} v_F^2 \sum_{n \geq 0} \left\{ N_+ \frac{\omega_n^2 - 2H_q^2}{(\omega_n^2 + H_q^2)^{5/2}} + N_- \frac{\omega_n^2 - 2H_{-q}^2}{(\omega_n^2 + H_{-q}^2)^{5/2}} \right\} \quad (\text{A.16})$$

$$\kappa_{2x} = \frac{\pi T}{8} v_F^2 \sum_{n \geq 0} \left\{ N_- \frac{\omega_n^2 - 2H_q^2}{(\omega_n^2 + H_q^2)^{5/2}} + N_+ \frac{\omega_n^2 - 2H_{-q}^2}{(\omega_n^2 + H_{-q}^2)^{5/2}} \right\} \quad (\text{A.17})$$

$$\kappa_{1y} = \frac{\pi T}{8} v_F^2 \sum_{n \geq 0} \left\{ \frac{N_+}{(\omega_n^2 + H_q^2)^{3/2}} + \frac{N_-}{(\omega_n^2 + H_{-q}^2)^{5/2}} \right\} \quad (\text{A.18})$$

$$\kappa_{2y} = \frac{\pi T}{8} v_F^2 \sum_{n \geq 0} \left\{ \frac{N_-}{(\omega_n^2 + H_q^2)^{3/2}} + \frac{N_+}{(\omega_n^2 + H_{-q}^2)^{5/2}} \right\} \quad (\text{A.19})$$

where $H_q = H - qv_F/2$, $H_{-q} = H + qv_F/2$, and v_F is the Fermi velocity (note that this is equal for helicity bands).

Appendix B: Properties of the Ginzburg-Landau model

Because the coefficients in front of the kinetic term are different, $\kappa_{ax} \neq \kappa_{ay}$, the Ginzburg-Landau model (1) is

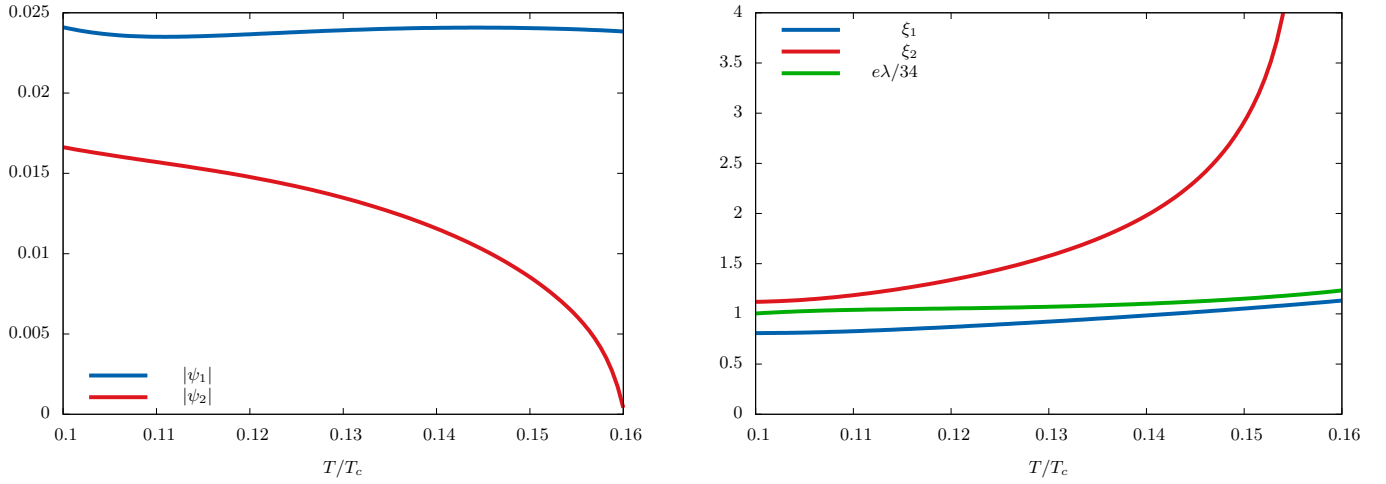


FIG. 5. (Color online) – The left panel shows the ground state densities, while the right panel displays the length scales as a function of temperature. Here the critical temperature T_c , denotes the upper phase transition where superconductivity disappears. The regime we are interested in, the multiple- Q phase, appears below $T/T_c \approx 0.16$ when the component the second component develops a non-zero ground state density.

anisotropic. To analyze the properties of the Ginzburg-Landau model, it is convenient to absorb the anisotropies by rescaling the fields and spatial coordinates. First, note that we take the prefactors of the kinetic to satisfy the relation $\kappa_{1y}/\kappa_{1x} = \kappa_{2y}/\kappa_{2x}$ which is numerically found to be accurate to 10^{-4} . The anisotropies are absorbed using the following parametrization

$$\begin{cases} \kappa_{1x} = \kappa_1/2 \\ \kappa_{1y} = m^2\kappa_1/2 \end{cases} \quad \begin{cases} \kappa_{2x} = \delta\kappa_{1x} \\ \kappa_{2y} = \delta\kappa_{1y} \end{cases}. \quad (\text{B.1})$$

The rescaled (isotropic) spatial coordinates are

$$\tilde{x} = x/\sqrt{\kappa_1}, \quad \tilde{y} = y/m\sqrt{\kappa_1}, \quad (\text{B.2})$$

and the rescaled fields

$$\begin{aligned} \tilde{A}_x &= A_x/m\sqrt{\kappa_1}, & \tilde{A}_y &= A_y/\sqrt{\kappa_1}, \\ \psi_1 &= \Delta_q, & \psi_2 &= \sqrt{\delta}\Delta_{-q}. \end{aligned} \quad (\text{B.3})$$

Defining the new parameters of the interacting potential

$$\begin{aligned} \tilde{\alpha}_1 &= \alpha_1, \quad \tilde{\beta}_1 = \beta_1, \\ \tilde{\alpha}_2 &= \frac{\alpha_2}{\delta}, \quad \tilde{\beta}_2 = \frac{\beta_2}{\delta^2}, \\ \tilde{\gamma} &= \frac{\beta_m}{\delta}, \quad \tilde{e} = 2em\kappa_1, \end{aligned} \quad (\text{B.4})$$

and defining the rescaled free energy $\tilde{\mathcal{F}} = m\kappa_1 f$, the Ginzburg-Landau model (1) now reads (now on we omit the \sim symbols)

$$\begin{aligned} \mathcal{F} &= \frac{1}{2}\mathbf{B}^2 - B_z H_z \\ &+ \sum_a \left\{ \frac{1}{2} |(\nabla + ie\mathbf{A})\psi_a|^2 + \alpha_a |\psi_a|^2 + \frac{1}{2}\beta_a |\psi_a|^4 \right\} \\ &+ \gamma |\psi_1|^2 |\psi_2|^2, \end{aligned} \quad (\text{B.5})$$

and the magnetic field is $\mathbf{B} = \nabla \times \mathbf{A}$. Functional variation of the free energy functional (B.5) determines the Euler-Lagrange equations of motion. That is, variation with respect to complex fields ψ_a^* gives the Ginzburg-Landau equation for the condensates, while variation with respect to the vector potential defines the Ampère's law

$$\begin{aligned} \mathbf{D}\mathbf{D}\psi_a &= 2 \frac{\partial V(\Psi)}{\partial \psi_a^*}, \quad \nabla \times \mathbf{B} + \mathbf{J} = 0, \\ \text{and } \mathbf{J} &\equiv \sum_a \mathbf{J}^{(a)} = \sum_a e \text{Im}(\psi_a^* \mathbf{D}\psi_a), \end{aligned} \quad (\text{B.6})$$

where the covariant derivative is $\mathbf{D} \equiv \nabla + ie\mathbf{A}$. The ground state is the state with constant densities of the superconducting condensates $|\psi_a| = u_a$, while \mathbf{A} is a pure gauge that can be chosen to be zero. The ground state densities should satisfy

$$\begin{cases} (\alpha_1 + \beta_1 u_1^2 + \gamma u_2^2) u_1 = 0 \\ (\alpha_2 + \beta_2 u_2^2 + \gamma u_1^2) u_2 = 0 \end{cases} \quad (\text{B.7})$$

The ground states are defined up to arbitrary global phase, that can be set to zero without loss of generality since the free energy (B.5) is invariant under global $U(1) \times U(1)$ transformation. Provided $\beta_1\beta_2 - \gamma^2 > 0$ and $\alpha_1, \alpha_2 < 0$, both ground state densities u_1, u_2 are non-zero:

$$u_1^2 = \frac{\alpha_2\gamma - \alpha_1\beta_2}{\beta_1\beta_2 - \gamma^2}, \quad u_2^2 = \frac{\alpha_1\gamma - \alpha_2\beta_1}{\beta_1\beta_2 - \gamma^2}. \quad (\text{B.8})$$

The condition $\beta_1\beta_2 - \gamma^2 > 0$ is a necessary condition both condensates to have non zero ground state and $\alpha_1, \alpha_2 < 0$ is the stability condition of the ground state. Both are verified for the range of temperature we considered.

The length scales at which a perturbed condensate recovers its ground state density, the coherence lengths ξ_a ,

are determined by expanding the fields around ground state $\psi_a = u_a + \epsilon_a$ and linearising the equations of motion (B.6). The length scales are determined by the eigenvalues \mathcal{M}_a^2 of the mass matrix

$$\mathcal{M}^2 = \begin{pmatrix} \alpha_1 + 3\beta_1 u_1^2 + \gamma u_2^2 & 2\gamma u_1 u_2 \\ 2\gamma u_1 u_2 & \alpha_2 + 3\beta_2 u_2^2 + \gamma u_1^2 \end{pmatrix}, \quad (\text{B.9})$$

and the coherence lengths are $\xi_a = 1/\sqrt{2\mathcal{M}_a^2}$ while the penetration depth is $e\lambda = 1/\sqrt{u_1^2 + u_2^2}$. The ground state densities and length scales, for the values of the Ginzburg-Landau potential parameters derived from the microscopic calculations, are displayed in Fig. 5.

Note that the coherence lengths ξ_1 and ξ_2 are not the coherence lengths associated with each condensates independently. Indeed, the modes here are hybridized. That is, ξ_1 and ξ_2 are the coherence lengths associated to orthogonal linear combinations of the fields ψ_1 and ψ_2 . These linear combinations form the eigenbasis of the mass matrix (B.9).

Flux quantization and fractional vortices

The elementary topological excitations, when several condensates are involved, are fractional vortices. These are field configurations with 2π phase winding of only one condensate. For example, φ_1 has $\oint \nabla \varphi_1 = 2\pi$ winding while $\oint \nabla \varphi_2 = 0$. A fractional vortex in the condensate a , carries only a fraction of flux quantum. This can be seen by calculating the magnetic flux. The supercurrent, defined from the equations of motion (B.6), reads as

$$\mathbf{J}/e := \frac{\delta \mathcal{F}}{\delta \mathbf{A}} = e\varrho^2 \mathbf{A} + \sum_a |\psi_a|^2 \nabla \varphi_a. \quad (\text{B.10})$$

Here we defined the total density $\varrho^2 = \sum_a |\psi_a|^2$. Since the supercurrent \mathbf{J} is screened, it decays exponentially and there, the condensates have constant density. The magnetic flux thus reads as

$$\begin{aligned} \Phi &= \frac{1}{e^2 \varrho^2} \oint \left(\mathbf{J} - e \sum_a |\psi_a|^2 \nabla \varphi_a \right) \cdot d\boldsymbol{\ell} \\ &= -\frac{\sum_a |\psi_a|^2}{e\varrho^2} \oint \nabla \varphi_a \cdot d\boldsymbol{\ell}. \end{aligned} \quad (\text{B.11})$$

Each condensate must wind an integer number of times. Thus, if ψ_1 winds n_1 times and ψ_2 winds n_2 times, the flux reads as [24]

$$\Phi = n_1 \frac{|\psi_1|^2 \Phi_0}{|\psi_1|^2 + |\psi_2|^2} + n_2 \frac{|\psi_2|^2 \Phi_0}{|\psi_1|^2 + |\psi_2|^2}, \quad (\text{B.12})$$

where the flux quantum is $\Phi_0 = 2\pi/e$. Fractional vortices in different condensates attract each other logarithmically at long distances. If $n_1 = n_2$, the two fractions $\frac{|\psi_a|^2}{|\psi_1|^2 + |\psi_2|^2}$ of flux add up to give integer flux. Restoring the original unit system gives the flux Eq. (2) of the main text.

Topology

Vortices, either fractional or composite are characterized by $S^1 \rightarrow S^1$ topological maps. The first circle S^1 denotes the closed path faraway from the vortex core (that is homeomorphic to a circle) while the second one (the target circle) correspond to $U(1)$ rotations. Heuristically the $S^1 \rightarrow S^1$ maps has the following meaning: they count how many times the target circle is covered while going along the closed path faraway from the vortex core. That is the number of phase windings. Importantly, this number can be calculating just by inspecting the closed path faraway for the vortex core. This is because the associated density of the topological invariant is a total divergence.

There are two kinds of field configurations that carry an integer number of flux quanta. Ordinary vortices, for which the two components winds around the same point, and skyrmions for which for which the two components do not wind around the same point. In the model which we derived these can continuously be deformed into each other at finite free energy cost. And one kind of topological defect is unstable against decaying into another. The vortices and skyrmions can be distinguished on topological grounds, by the topological invariant associated with $S^2 \rightarrow S^2$ topological maps. The first S^2 here stands for the compactification of the \mathbb{R}^2 plane. Heuristically this topological map counts the number of times the target sphere (defined below as the projection of the condensates on Pauli matrices), is covered while covering the plane \mathbb{R}^2 . Note that here the density of topological invariant associated with this map is not a total divergence (see Eq. (B.13)). Thus the topological invariant, which cannot be reduced to a line integral, is clearly different from that of the $S^1 \rightarrow S^1$ maps. The topological invariant is rigorously derived by defining Ψ , the vector of complex fields: $\Psi^\dagger = (\psi_1^*, \psi_2^*)$. Ψ is a smooth holomorphic map $M \rightarrow \mathbb{C}^2$ with the manifold M denoting the infinite plane \mathbb{R}^2 . Note that M can also stand for the one-point compactification of the plane which is homeomorphic to a sphere $M = \mathbb{R}^2 \cup \{\infty\} \simeq S^2$. Now, we define the projection $\pi : \mathbb{C}^2 \setminus \{0\} \rightarrow \mathbb{C}P^1$, which is roughly speaking the stereographic projection. Then $\phi = \pi \circ \Psi$ is a $\mathbb{C}P^1$ -valued field that maps all point in M to a point in $\mathbb{C}P^1$. This has topological degree $\mathcal{Q}(\Phi) = \frac{1}{4\pi} \int_M \phi^* \omega \in \mathbb{Z}$, where ω is the Kähler form associated with the Fubini-Study metric on $\mathbb{C}P^1$. The topological index \mathcal{Q} can be rewritten in term of the complex field Ψ as

$$\mathcal{Q}(\Psi) = \int_M \frac{i\epsilon_{ji}}{2\pi|\Psi|^4} [|\Psi|^2 \partial_i \Psi^\dagger \partial_j \Psi + \Psi^\dagger \partial_i \Psi \partial_j \Psi^\dagger \Psi] d^2 x, \quad (\text{B.13})$$

and \mathcal{Q} equals the number of enclosed flux quanta ($2\pi\mathcal{Q}/e = \int_M B dS$), provided $\Psi \neq 0$. For a more complete, rigorous and detailed demonstration, see the demonstration for an arbitrary number of complex fields in [34]. The $\mathbb{C}P^1$ topological invariant (B.13) for skyrmions can alternatively be derived using the pseudo-

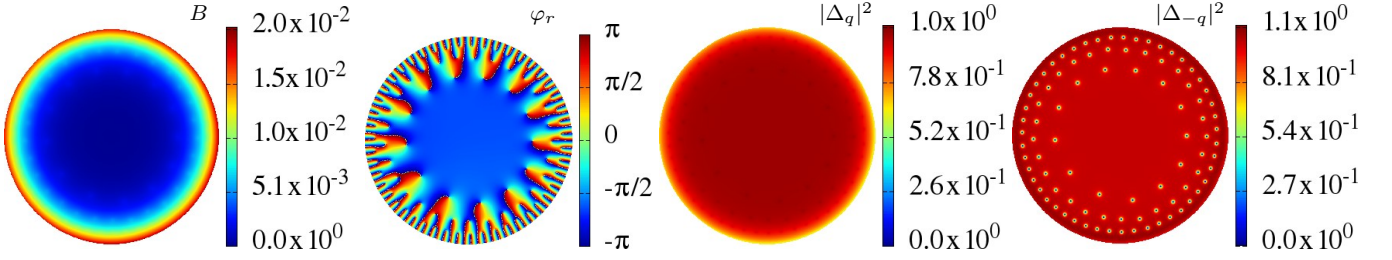


FIG. 6. (Color online)– Near boundary stable fractional vortices. Displayed quantities are the magnetic field B (in units of H_{c2}), the condensate densities in the units of their ground state value, and the relative phase between both condensates $\varphi_r := \varphi_- - \varphi_+$. The spatial coordinates x and y are scaled units of $\sqrt{2\kappa_{1x}}$ and $\sqrt{2\kappa_{1y}}$ respectively. Vortices enter in the Δ_{-q} condensate, while no vortices enter in Δ_q . This can be seen from the phase difference, where winding in φ_r indicates the existence of fractional vortices. Quite remarkably, there are several layers of stable fractional vortices near the boundary. Here the applied field is strong enough to allow many (weak) vortices in Δ_{-q} to enter, but not strong enough so that vortices in Δ_q can overcome the Bean-Livingstone barrier. If there are a few fractional vortices, they would stay in a single layer that is closest to the boundary. However, since there are so much fractional vortices, the system has to compromise and put multiple layers of fractional vortices.

spin \mathbf{n} . That derivation, more known in several area of physics, is equivalent to the derivation we used for (B.13). The pseudo-spin unit vector \mathbf{n} is the projection of superconducting condensates on spin-1/2 Pauli matrices $\boldsymbol{\sigma}$:

$$\mathbf{n} \equiv (n_x, n_y, n_z) = \frac{\Psi^\dagger \boldsymbol{\sigma} \Psi}{\Psi^\dagger \Psi}, \quad \text{where } \Psi^\dagger = (\psi_1^*, \psi_2^*). \quad (\text{B.14})$$

Roughly speaking this is the stereographic projection π mentioned earlier. The pseudo-spin is a map from the one-point compactification of the plane ($\mathbb{R}^2 \simeq S^2$) to the two-sphere target space spanned by \mathbf{n} . That is $\mathbf{n} : S^2 \rightarrow S^2$, and this map is characterized by the homotopy class $\pi_2(S^2) \in \mathbb{Z}$, thus defining the integer valued topological (skyrmionic) charge

$$\mathcal{Q}(\mathbf{n}) = \frac{1}{4\pi} \int_{\mathbb{R}^2} \mathbf{n} \cdot \partial_x \mathbf{n} \times \partial_y \mathbf{n} \, dx dy. \quad (\text{B.15})$$

The key point in both these derivations (B.13) and (B.15) of the integer topological invariant \mathcal{Q} , is that it relies on the fact that $\Psi \neq 0$. That is it is integer only if ψ_1 and ψ_2 have no coincident cores. In other words, ordinary (composite) vortices with a single core $\Psi = 0$, have $\mathcal{Q} = 0$. Skyrmions (core-split vortices), on the other hand, have non-trivial charge $\mathcal{Q} = N$ (with N coincides with the number of carried flux quanta). Note that when $\Psi \neq 0$, \mathcal{Q} is an integer provided the fields recover ground state at the boundary of the integration domain. This means that, for example, Meissner currents make this definition for \mathcal{Q} non integer.

Appendix C: Additional detail

Here, we give additional details about regimes discussed in the main body paper. Fig. 6 shows stable fractional vortices near boundary. This is for the same parameters as in Fig. 2 the paper, but for higher applied field. The applied field exceeds H_{c1} , but it is insufficient

to overcome Bean-Livingston barrier for entry of vortices in Δ_q . As a result, fractional vortices enter Δ_{-q} and sit near boundary since they have divergent energy and are unstable in bulk system. The applied field here is larger than in Fig. 2 of the paper. As a result, many more vortices enter Δ_{-q} . Since fractional vortices repel each other, the system compromises by creating multiple layers of fractional vortices, instead of forming a single layer. This is consistent with theoretical calculations in a general two-component London model [25].

Fig. 7 shows the temperature evolution of the skyrmion lattice displayed in Fig. 3 of the paper. As temperature is decreased, the skyrmion lattice first formed is very regular. In particular, close to $H_{c2}^{(-q)}$, the two condensates form triangular lattices, with one lattice displaced relative to the other. The displacement is such that vortices of Δ_{-q} lie in the center of a triangle of vortices in Δ_q . For reduced values of the temperature, vortices in Δ_{-q} no longer sit in the center of triangles of vortices in Δ_q . A vortex in Δ_{-q} pairs with one of the three surrounding vortices of Δ_q and the resulting skyrmion lattice is no longer triangular. As the system is further cooled, the individual skyrmions become increasingly less separated and eventually merge into usual vortices. Finally, the lattice has thus collapsed into a triangular lattice of Abrikosov vortices.

Appendix D: Numerical methods

We consider the two-dimensional problem (B.5), defined on the domain $\Omega \subset \mathbb{R}^2$ bounded by $\partial\Omega$. In our simulations, we choose Ω to be a disc. The problem is supplemented by the boundary condition $\mathbf{n} \cdot \mathbf{D}\psi_a = 0$ with \mathbf{n} the normal vector to $\partial\Omega$. Physically this condition implies there is no current flowing through the boundary. The external field applied field $\mathbf{H} = H_z \hat{z}$ yields the boundary conditions on $\partial\Omega$ for the vector potential $\nabla \times \mathbf{A} = \mathbf{H}$.

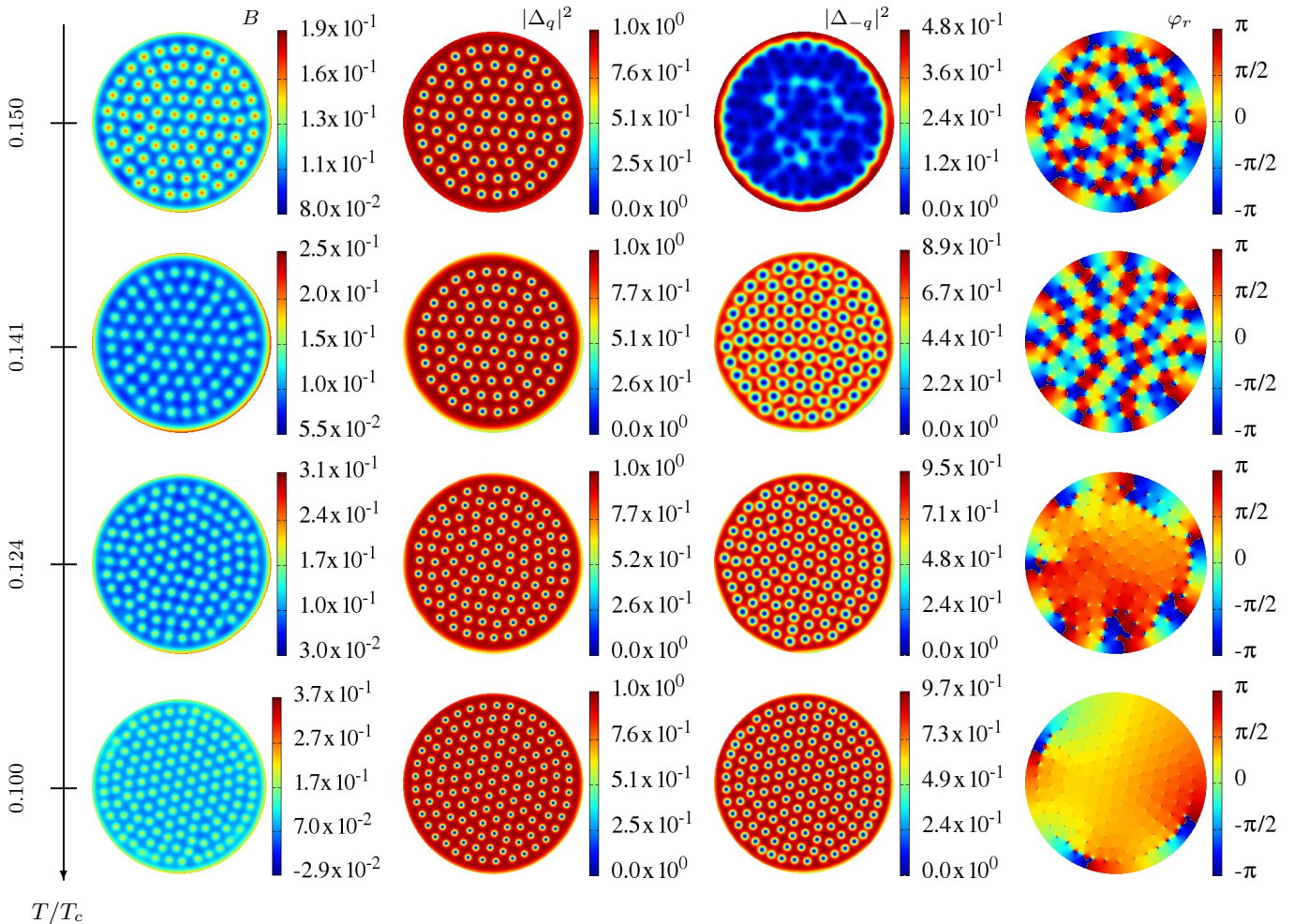


FIG. 7. (Color online) – Transition from a skyrmion lattice state to a vortex lattice state as temperature is decreased. This shows the magnetic field B (in units of H_{c2}), the condensate densities in the units of their ground state value, and the relative phase $\varphi_r = \varphi_- - \varphi_+$ between both condensates Δ_q and Δ_{-q} . The spatial coordinates x and y are scaled units of $\sqrt{2\kappa_{1x}}$ and $\sqrt{2\kappa_{1y}}$ respectively. Here, the applied field exceeds the second critical field associated with the (weak) component Δ_{-q} . As a result, at $T/T_c = 0.16$, Δ_{-q} is completely suppressed. On the other hand, the field is strong enough for the component Δ_q to develop a regular triangular vortex lattice (here it is not perfect because the circular boundary causes disclinations in the lattice). As the temperature is decreased, Δ_{-q} develops superconductivity accompanied with many vortices. In this regime, close the second critical field associated with the (weak) component Δ_{-q} , the lattice in Δ_{-q} does not superimpose with that in Δ_q . This can be seen by the relative phase φ_r of the two condensates. With cooling further, as the Δ_{-q} becomes larger, the skyrmion lattice is no more favoured and vortices in both components tend to overlap. At the lowest temperatures, all vortices are co-centred and form a triangular lattice, apart from three extra fractional vortices in Δ_{-q} that are in a (meta-)stable near boundary configuration.

The variational problem is defined for numerical computation using a finite element formulation provided by the **Freefem++** library [35]. Discretization within finite element formulation is done via a (homogeneous) triangulation over Ω , based on the Delaunay-Voronoi algorithm. Functions are decomposed on a continuous piecewise quadratic basis over each triangle. The accuracy of such a method is controlled through the number of triangles, (we typically used $3 \sim 6 \times 10^4$), the order of expansion of the basis on each triangle (second order polynomial basis on each triangle). A numerical optimization algorithm (non-linear conjugate gradient) is then used to solve the variational non-linear problem. The algorithm

is iterated until relative variation of the norm of the gradient of the functional \mathcal{G} with respect to all degrees of freedom is less than 10^{-8} .

In our simulations, we focused on simulations that reproduce field cooled experiments. That is, we start at $T/T_c = 0.16$, the temperature of the transition between single- Q and the multiple- Q phase when no normal field is applied. We select a value of the applied field H_z . We then minimize the free energy until convergence for a given temperature. For the next step the temperature is decreased by step $dT = 10^{-3}$ and the free energy is subsequently minimized using the solution at the previous temperature as a starting point. This procedure is

iterated down to the final temperature, $T_{min} = 0.1T_c$.

-
- [1] T. D. Stanescu, B. Anderson, and V. Galitski, *Phys. Rev. A* **78**, 023616 (2008).
 - [2] Y.-J. Lin, K. Jimenez-Garcia, and I. B. Spielman, *Nature* **471**, 83 (2011).
 - [3] C. Wang, C. Gao, C.-M. Jian, and H. Zhai, *Phys. Rev. Lett.* **105**, 160403 (2010).
 - [4] P. Fulde and R. A. Ferrell, *Phys. Rev.* **135**, A550 (1964).
 - [5] A. Larkin and Y. Ovchinnikov, *Sov. Phys. JETP* **20**, 762 (1965).
 - [6] O. Dimitrova and M. V. Feigel'man, *Phys. Rev. B* **76**, 014522 (2007).
 - [7] D. F. Agterberg, Z. Zheng, and S. Mukherjee, *Phys. Rev. Lett.* **100**, 017001 (2008).
 - [8] L. Radzihovsky and A. Vishwanath, *Phys. Rev. Lett.* **103**, 010404 (2009).
 - [9] L. Radzihovsky, *Physica C* **481**, 189 (2012).
 - [10] S. Gopalakrishnan, J. C. Y. Teo, and T. L. Hughes, *Phys. Rev. Lett.* **111**, 025304 (2013).
 - [11] E. Berg, E. Fradkin, E.-A. Kim, S. A. Kivelson, V. Oganesyan, J. M. Tranquada, and S. C. Zhang, *Phys. Rev. Lett.* **99**, 127003 (2007).
 - [12] D. F. Agterberg and H. Tsunetsugu, *Nat. Phys.* **4**, 639 (2008).
 - [13] E. Berg, E. Fradkin, S. A. Kivelson, and J. M. Tranquada, *New J. Phys.* **11**, 115004 (2009).
 - [14] E. Babaev, *Nuclear Physics B* **686**, 397 (2004).
 - [15] E. Berg, E. Fradkin, and S. A. Kivelson, *Nat. Phys.* **5**, 830 (2009).
 - [16] D. F. Agterberg, M. Geracie, and H. Tsunetsugu, *Phys. Rev. B* **84**, 014513 (2011).
 - [17] A. Ohtomo and H. Y. Hwang, *Nature* **427**, 423 (2004).
 - [18] N. Reyren, S. Thiel, A. D. Caviglia, L. F. Kourkoutis, G. Hammerl, C. Richter, C. W. Schneider, T. Kopp, A.-S. Rüetschi, D. Jaccard, M. Gabay, D. A. Muller, J.-M. Triscone, and J. Mannhart, *Science* **317**, 1196 (2007).
 - [19] K. Ueno, S. Nakamura, H. Shimotani, A. Ohtomo, N. Kimura, T. Nojima, H. Aoki, Y. Iwasa, and M. Kawasaki, *Nat. Mater.* **7**, 855 (2008).
 - [20] K. Ueno, S. Nakamura, H. Shimotani, H. T. Yuan, N. Kimura, T. Nojima, H. Aoki, Y. Iwasa, and M. Kawasaki, *Nat. Nano.* **6**, 408 (2011).
 - [21] K. Taniguchi, A. Matsumoto, H. Shimotani, and H. Takagi, *Appl. Phys. Lett.* **101**, 042603 (2012).
 - [22] J. T. Ye, Y. J. Zhang, R. Akashi, M. S. Bahramy, R. Arita, and Y. Iwasa, *Science* **338**, 1193 (2012).
 - [23] D. F. Agterberg and R. P. Kaur, *Phys. Rev. B* **75**, 064511 (2007).
 - [24] E. Babaev, *Phys. Rev. Lett.* **89**, 067001 (2002).
 - [25] M. A. Silaev, *Phys. Rev. B* **83**, 144519 (2011).
 - [26] G. Eilenberger, *Zeitschrift für Physik* **214**, 195 (1968).
 - [27] J. Serene and D. Rainer, *Physics Reports* **101**, 221 (1983).
 - [28] D. Agterberg, *Physica C* **387**, 13 (2003).
 - [29] V. Moshchalkov, M. Menghini, T. Nishio, Q. H. Chen, A. V. Silhanek, V. H. Dao, L. F. Chibotaru, N. D. Zhigadlo, and J. Karpinski, *Phys. Rev. Lett.* **102**, 117001 (2009).
 - [30] S. J. Ray, A. S. Gibbs, S. J. Bending, P. J. Curran, E. Babaev, C. Baines, A. P. Mackenzie, and S. L. Lee, *Phys. Rev. B* **89**, 094504 (2014).
 - [31] E. Babaev and M. Speight, *Phys. Rev. B* **72**, 180502 (2005).
 - [32] J. Carlström, E. Babaev, and M. Speight, *Phys. Rev. B* **83**, 174509 (2011).
 - [33] A. Larkin and Y. Ovchinnikov, *Sov. Phys. JETP* **28**, 1200 (1969).
 - [34] J. Garaud, J. Carlström, E. Babaev, and M. Speight, *Phys. Rev. B* **87**, 014507 (2013).
 - [35] F. Hecht, *J. Numer. Math.* **20**, 251 (2012).